Journal of Engineering Mechanics and Machinery (2025)
Clausius Scientific Press, Canada

DOI: 10.23977/jemm.2025.100104
ISSN 2371-9133 Vol. 10 Num. 1

Research on the Engineering Mechanics Equations of a Pipeline Robot Supported by Wheel Systems

Xiaomin Shan

College of Engineering, Inner Mongolia Minzu University, Tongliao, Inner Mongolia Autonomous Region, China
135351125@qq.com

Keywords: Support Wheel Robot; Oil Pipeline; Mechanical Model; Motion Control; Stability

Abstract: Existing oil pipeline robots generally face stability and adaptability problems in complex terrain and different environmental conditions. Especially under high load and complex pipeline paths, the robot's motion control and mechanical response often cannot meet the requirements. To this end, this paper first constructs a mechanical model of a supported wheeled robot in a pipeline environment. By analyzing the response of the robot under different terrain and disturbance conditions, a set of control methods based on dynamic optimization are proposed. This paper accurately calculates the contact force and motion trajectory of the robot on the pipeline by establishing a multi-factor coupling model including normal force, tangential force and friction force, and simulates and verifies its performance under different operating conditions. The study also deeply analyzes the dynamic response of the robot under speed and slope conditions to ensure its efficient movement in difficult environments. The experimental results show that the robot's motion control accuracy has been significantly improved through the improved mechanical model, especially in pipeline environments with high-speed movement and complex slopes. Under flat conditions, the robot has a recovery time of 2.1 seconds after being disturbed by a speed of 0.5 m/s, a maximum displacement deviation of 0.15 meters, and a maximum posture deviation of 3.5°.

1. Introduction

As an important energy transmission channel, oil pipelines are widely used around the world. However, due to the long distance, complex terrain and harsh environment, the safety and operational stability of pipelines face huge challenges. Traditional manual inspections and conventional equipment often have problems such as low efficiency, poor reliability and high operational risks in these harsh environments. Therefore, the development of efficient, safe and intelligent pipeline robots has become the key to improving the efficiency of pipeline monitoring and maintenance.

Although the supported wheeled robot has certain advantages in design, how to optimize its mechanical properties and motion control for different terrains, different pipeline environments and external disturbance conditions is still an urgent problem to be solved. In order to make up for the

shortcomings of existing robots in these aspects, this paper proposes a new research method for supported wheeled oil pipeline robots based on engineering mechanics equations, aiming to improve the stability and adaptability of the robot in complex environments through precise modeling and mechanical analysis.

This paper first introduces the challenges faced by oil pipeline robots, proposes the potential of supported wheeled robots as a solution, and clarifies the research objectives and methods. Then, the mechanical model of the supported wheeled robot is constructed in detail, the coupling relationship between factors such as normal force, tangential force and friction force is analyzed, and the relevant dynamic equations are derived. Subsequently, the effectiveness of the model is verified through experiments and simulations, and the performance of the robot under different terrain and disturbance conditions is demonstrated. Finally, the research results are summarized and the future application direction in the field of intelligent pipeline inspection is prospected.

2. Related Work

In order to cope with the increasingly complex robot control problems, many scholars have proposed different control strategies and methods in recent years to improve the performance and stability of robot systems. Nekoo et al. proposed a new terminal sliding mode control method to control a class of nonlinear uncertain systems and ensure that the control task is completed within a finite time. This control method defines the final time by introducing a finite time gain and solves the gain using the state-related differential Riccati equation [1]. Seghiri et al. proposed an adaptive control design based on a fractional-order model reference adaptive control strategy. Compared with the traditional adaptive control strategy, this scheme used a fractional-order system as a reference model and introduced a fractional-order integrator to adjust the parameters [2]. Semwal et al. proposed a gait generation learning method based on a long short-term memory model to overcome the instability problem of the model method in the process of optimizing boundary conditions and mass inertia parameters [3]. Armanini et al. first conducted a structured review of existing soft robot modeling methods, classified them according to their theoretical and numerical foundations, and provided a critical analysis [4]. Briot and Merle proved that the static configuration of the drooping CDPR (cable-driven parallel robots) is a local extremum of the function describing the robot's potential energy, and proposed to evaluate the stability by checking the Legendre–Clebsch condition and Jacobi condition. The simulation results were verified by the stability of the convergent model [5]. Kadhim et al. obtained the dynamic equations of the two-link robot arm through the Lagrangian method, and the adjustment coefficients of the controller were solved by the optimization problem, and the optimal coefficients were determined by the honey bee algorithm optimization technique [6]. Ahmadizadeh et al. derived the dynamic equations of an open-chain robot system and obtained the equations of a closed-loop system through constraints. They used a contact force model to simulate impact contact and considered the effect of friction on collision [7]. Khorashadizadeh et al. designed a simple tracking controller for a robot manipulator driven by a permanent magnet synchronous motor using an orthogonal function method. The orthogonal function was used to estimate and compensate for the uncertainties in the system, including external disturbances and system dynamics. The results showed that the control method was superior to traditional methods in tracking performance and had a lighter computational burden [8]. Lanh et al. proposed a method combining model reference adaptive control and backstepping algorithm to solve the parameter uncertainty problem in the control of the lower limbs of a humanoid robot driven by a passive compliant series elastic actuator. Experimental results showed that the control algorithm was effective [9]. Li et al. proposed a strictly predefined-time convergent and noise-tolerant zeroing neural network (SPTC-NT-ZNN) to solve time-varying linear equations,

which is particularly suitable for time-sensitive applications. By comparing with the typical ZNN model, SPTC-NT-ZNN performed better in terms of convergence and robustness [10]. Barbosa et al. proposed a novel method for planning the motion of a fish-like soft robot driven by macro-fiber composite materials. The method simulated the oscillatory and wave motion of fish by making the tail movement amplitude larger than the head movement amplitude, and ensured the appropriate structural modal shape through the design strategy of centralized and distributed mass [11]. Chotikunnan et al. developed a robot arm control system using MATLAB/Simulink and Arduino microcontroller. The robot armed consists of three motors and adjustable resistors, and was connected to MATLAB/Simulink software through an Arduino microcontroller to control position and rotation in real time. The experimental results showed that the errors of the robot arm on the A, B, and C motor axes were 2.8587, 5.7340, and 4.4406, respectively [12]. Although existing research has made significant progress in the field of robot control, many methods still face limitations in practical applications, such as dealing with uncertainties in complex environments, dynamic changes in parameters, and stability issues under high precision requirements.

3. Method

3.1 System Modeling and Mechanical Analysis

3.1.1 Description of the structure of a wheeled robot

The wheeled robot is mainly composed of a body, support wheels, drive system, sensors, etc. The body is usually a rigid frame that carries all electronic equipment, power systems, and support wheels. The support wheels are the key part of the robot in contact with the ground, supporting its weight and providing the necessary stability. According to the arrangement of the support wheels, there are many types of wheeled robots, such as single-wheel drive, dual-wheel drive, or multi-wheel drive.

The main function of the support wheel is to bear the weight of the robot and keep it in contact with the ground during movement. The design of the support wheel needs to meet the requirements of load capacity, friction, durability, flexibility, etc. Common types of support wheels include omnidirectional wheels, standard track wheels, and directional wheels.

3.1.2 Mechanical model of support wheel and ground contact

The contact relationship between the support wheel and the ground is a key issue in the robot motion and stability analysis. The contact between the support wheel and the ground is usually regarded as a nonlinear contact problem, in which the distribution of friction, normal force and tangential force plays a decisive role in the robot's motion performance and stability.

(1) Friction model

Friction is the main force when the support wheel contacts the ground. The magnitude and direction of friction are closely related to the roughness of the support wheel surface, the material of the tire, and the ground conditions. Commonly used friction models include the Coulomb friction model and the extended Coulomb model, the latter of which takes into account the change of the dynamic friction coefficient.

(2) Normal force

Normal force is the vertical force generated when the support wheel contacts the ground. It is usually the combined effect of the weight of the robot and any external load. In static conditions, the normal force is equal to the gravity acting on the robot. In dynamic conditions, the normal force varies depending on the relative motion between the wheel and the ground.

(3) Tangential force

The tangential force is the force that causes the support wheels to slide or roll along the ground surface. This force is affected by friction and the robot's motion, and usually varies with speed. The effect of the tangential force is particularly significant at high speeds.

3.2 Derivation of Engineering Mechanics Equations for Supporting Wheeled Robots

3.2.1 Kinematic equations for supporting wheeled robots

The kinematic equations of a supported wheeled robot describe the robot's position, posture, and motion trajectory in space. Assuming that the robot is a rigid body consisting of multiple wheels, and the contact points between the wheels and the ground provide the support force for movement.

Coordinate system selection: In a general supported wheeled robot, the global coordinate system $O-XYZ$ and the local coordinate system $o-x_o y_o z_o$ are selected. The robot's motion relative to the global coordinate system can be described by the transformation of the local coordinate system.

Plane kinematic equation: Assuming that the robot moves in a plane and only involves translation and rotation, its kinematic equation can be expressed as:

$$\dot{x} = v_x = R.\left(\sum_{i=1}^{n} w_i . r_i . \cos(\theta_i)\right) \tag{1}$$

$$\dot{y} = v_y = R.\left(\sum_{i=1}^{n} w_i . r_i . \sin(\theta_i)\right) \tag{2}$$

$$\dot{\theta} = w = \frac{1}{I} . \sum_{i=1}^{n} T_i \tag{3}$$

Among them:

x, y are the position of the robot in the global coordinate system; $\dot{x}, \dot{y}$ are the speed; θ is the angle of the robot's orientation; w is the angular velocity; w_i is the angular velocity of the i-th support wheel; r_i and θ_i are the distance and angle from the i-th support wheel to the robot's center of mass; I is the robot's moment of inertia, and T_i is the torque generated by the i-th wheel.

3.2.2 Analysis of external forces and inertial forces

During the movement of a wheeled robot, the effects of external forces and inertial forces cannot be ignored. External forces include friction, driving force, gravity, elastic force, and constraint force, while inertial forces are related to the robot's mass, speed, and acceleration.

External force analysis: The external force can be expressed as the resultant force of various forces acting on the robot, and its components in the robot's plane coordinate system are:

$$F_{ext} = F_{gravity} + F_{friction} + F_{applied} + F_{constraint} \tag{4}$$

Among them: $F_{gravity} = mg$ is gravity; $F_{friction} = \mu N$ is friction, where μ is the friction coefficient and N is the normal force; $F_{applied}$ is the externally applied force; and $F_{constraint}$ is the force due to motion constraints.

Inertia force analysis: The robot generates inertia force during movement. The magnitude of the inertia force is related to the robot's mass m, velocity v and acceleration a. The inertia force can be expressed as:

$$F_{inertia} = m.a \tag{5}$$

Among them, $a = \dot{v}$ is the acceleration and V is the velocity vector.

3.2.3 Stability analysis of robot motion

Stability analysis of robot motion is usually performed by linearizing the equations of motion, especially in the case of small disturbances. Stability analysis focuses on whether the robot can maintain its original motion state or return to a balanced state when subjected to external disturbances or dynamic changes.

Lyapunov stability criterion: The stability of the system is determined by defining the Lyapunov function $V(x)$ and checking the sign of its derivative $V(x)$. Assuming that the dynamic equation of the robot system is:

$$\dot{x} = f(x) \tag{6}$$

The derivative of the Lyapunov function is:

$$\dot{V}(x) = \nabla V(x).f(x) \tag{7}$$

If $\dot{V}(x) \leq 0$ and $\dot{V}(x) = 0$ only holds when $x = 0$, then the system is stable.

3.2.4 Degree of freedom analysis and constraints

Degree of freedom analysis is used to determine the number of independent movements a robot can make. In a supported wheeled robot, assuming the robot is a rigid body, its degrees of freedom f can be calculated using the following formula:

$$f = 6 - c \tag{8}$$

Among them, 6 is the total degrees of freedom in space and c is the number of constraints. Constraints typically include contact point constraints for the wheels, shape constraints for the ground or pipe, and other control input constraints.

3.2.5 Analysis of the impact of terrain and pipeline environment

The morphology of the pipeline surface (such as roughness, curvature, etc.) has a great impact on the operation of the supporting wheeled robot. The surface roughness directly affects the friction, thereby affecting the stability of the robot's driving. Pipes with large curvature may increase the lateral friction of the robot, making it more difficult to control.

For the friction force on the pipe surface, the following model can be used

$$F_{friction} = \mu.N \tag{9}$$

Among them, μ is the friction coefficient between the pipe surface and the wheel, and N is the normal force between the wheel and the pipe surface.

The mechanical response of the robot is different under different terrain conditions. Uneven ground, slope changes, and the presence of obstacles affect the robot's driving path and stability.

The effect of slope on the gravity component generated by the robot can be expressed by the following formula:

$$F_{gravity,slope} = m.g.\sin(\alpha) \tag{10}$$

Among them, α is the slope angle, m is the robot mass, and g is the gravitational acceleration.

3.3 Correction of the Motion Equation by Pipe Bending and Obstacles

When the robot travels in a curved pipe, the bending of the pipe causes the robot's motion state to change, thereby correcting its motion equation. The effect of the bending can be expressed by the following correction terms:

$$F_{curve} = m.\frac{v^2}{r} \tag{11}$$

Among them, r is the radius of curvature of the pipe and v is the speed of the robot.

The motion control model is used to describe the relationship between the robot's motion target, control input and output. Common control models include PID control, LQR control and model predictive control (MPC).

PID controller: The control input of the PID controller can be expressed by the following formula:

$$u(t) = K_p e(t) + K_i \int e(\tau) d_\tau + K_d \dot{e}(t) \tag{12}$$

Among them, $e(t)$ is the error between the desired position and the actual position, and K_p, K_i, and K_d are proportional, integral, and differential gains, respectively.

The optimization of mechanical equations is usually achieved by adjusting the control input and adjusting the system parameters to meet the design goals (such as maximizing efficiency, stability, etc.).

Optimization goal: The optimization problem can usually be expressed as:

$$\min J = \int_0^T (c_1.\left\|X(t) - X^*(t)\right\|^2 + c_2.\left\|u(t)\right\|^2)dt \tag{13}$$

Among them, $X(t)$ is the state of the system, $X^*(t)$ is the desired state, $u(t)$ is the control input, c_1 and c_2 are the weight coefficient.

3.4 Path Planning and Load Adaptability Optimization

Path planning aims to generate an efficient driving route for the robot, while load adaptability optimization focuses on how to adjust the robot parameters so that it can still maintain optimal performance under different load conditions. Commonly used path planning methods include A* algorithm, Dijkstra algorithm, and rapidly expanding random tree (RRT).

Load adaptability optimization: Load adaptability optimization optimizes performance by adjusting the robot's driving torque and the contact force of the support wheel. When the load changes, the control system needs to be adjusted in real time to ensure the stability of the robot.

4. Results and Discussion

4.1 Experimental Setup

Support wheeled robot (including multiple support wheels, drive system, sensors, etc.); environmental simulation system, including different terrains (flat ground, ramps, curved pipelines,

etc.); high-precision position sensors (such as lidar, cameras, etc.) for real-time acquisition of robot position information; force sensors for measuring the contact force between the robot and the ground or pipeline; control system to support the debugging of motion control and optimization algorithms; data recording system for collecting robot motion trajectory, speed, acceleration and other data.

4.2 Performance Test

Testing the robot's motion trajectory under different control inputs on flat ground and ramps to evaluate the deviation of its speed and acceleration from the expected values. Measuring the robot's position information and posture changes through sensors.

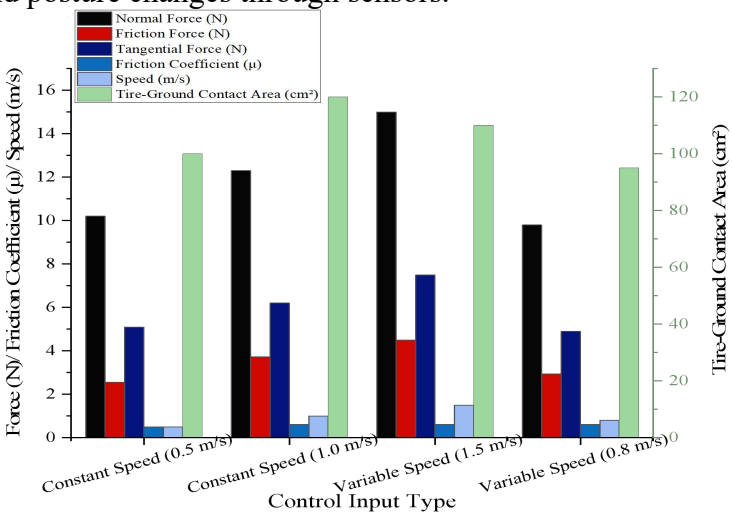

Figure 1. Friction and contact force test on rough surface

The experimental results in Figure 1 show that in the constant speed test, when the speed is 0.5 m/s, the normal force on the robot is 10.2 N, the tangential force is 5.1 N, the friction force is 2.55 N, and the friction coefficient is 0.5; when the speed increases to 1.0 m/s, the normal force increases to 12.3 N, the tangential force is 6.2 N, the friction force is 3.72 N, and the friction coefficient increases to 0.6. This shows that with the increase in speed, the friction and tangential force increase, and the friction coefficient also increases, indicating that the friction between the ground and the tire is strengthened. In the speed change test, when the robot is tested at a speed of 1.5 m/s, the normal force reached 15 N, the tangential force is 7.5 N, the friction force is 4.5 N, and the friction coefficient is 0.6, showing a higher friction and a stronger ground contact effect. In contrast, when the speed is reduced to 0.8 m/s, the normal force is 9.8 N, the tangential force is 4.9 N, the friction force dropped to 2.94 N, and the friction coefficient remained at 0.6, indicating that the change in speed has a more significant effect on the friction. Overall, the experimental results show that the speed change of the control input has a significant impact on the friction, normal force and friction coefficient. In particular, at high speeds, the friction and tangential forces are significantly increased, further strengthening the contact effect between the ground and the tire. In the friction and contact force tests on smooth surfaces, the experiment considered two control inputs: constant speed and variable speed. The results show that as the speed changes, the friction, normal force and friction coefficient between the robot and the ground also change significantly.

Under constant speed conditions, when the speed is 0.5 m/s, the normal force on the robot is 8.4 N, the tangential force is 3.5 N, the friction is 1.68 N, the friction coefficient is 0.5, and the tire-ground contact area is 110 cm². When the speed is increased to 1.0 m/s, the normal force increases to 10.1 N, the tangential force is 4.2 N, the friction is 2.1 N, and the friction coefficient

rises slightly to 0.52. This shows that as the speed increases, both the normal force and the friction force increase, and the friction coefficient also rises slightly, indicating that the friction effect is stronger at high speeds. In the variable speed test, when the speed is 1.5 m/s, the normal force reaches 12.2 N, the tangential force is 5.0 N, the friction force is 2.56 N, and the friction coefficient drops slightly to 0.51. When the speed is 0.8 m/s, the normal force is 6.7 N, the tangential force is 2.9 N, the friction force drops to 1.45 N, and the friction coefficient remains at 0.51 (as shown in Figure 2). The experimental results of variable speed show that higher speeds lead to greater friction and tangential forces, but the friction coefficient does not change significantly, indicating that the friction behavior of the robot is relatively stable at variable speeds.

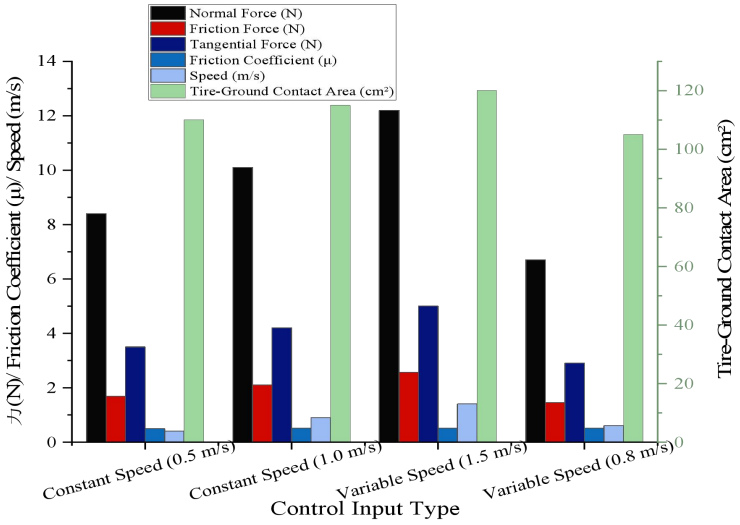

Figure 2. Friction and contact force test on smooth surface

By applying disturbances to the robot (such as a sudden change in direction or speed), observe its recovery process. Using the Lyapunov stability criterion or numerical simulation to analyze the stability of the robot when subjected to external disturbances.

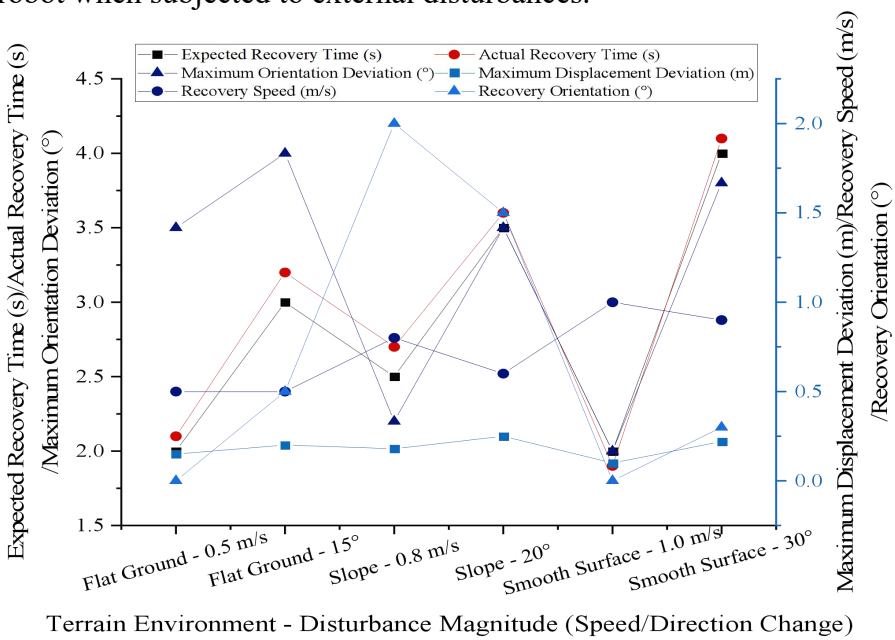

Figure 3. Robot stability test (recovery after disturbance)

Under flat conditions, after being disturbed by a speed of 0.5 m/s, the robot recovers in 2.1 seconds, with a maximum displacement deviation of 0.15 meters and a maximum posture deviation of 3.5°, showing a relatively stable recovery process. However, under complex terrain such as ramps and smooth surfaces, the robot's recovery time increases, especially in the case of large slopes. For example, in the experiment with a 20° slope, the robot recovers in 3.6 seconds, with a maximum displacement deviation of 0.25 meters and a posture deviation of 3.5°, showing that the ramp environment poses certain challenges to the robot's recovery ability. On flat ground and smooth surfaces, the robot can recover quickly and at a relatively stable speed. For example, under a disturbance of 1.0 m/s on a smooth surface, the robot's recovery speed reaches 1 m/s, and the posture angle after recovery is 0°. In the environment of a 30° slope, the recovery time is 4.1 seconds, with a lower recovery speed of about 0.9 m/s and a recovery posture of 0.3°, indicating that the robot's recovery ability is limited under large slopes (as shown in Figure 3).

In this experiment, the robot's stability in different terrain environments is tested, especially its ability to recover when subjected to speed or direction disturbances. The experiment includes three different terrains: flat ground, ramps, and smooth surfaces. The disturbance amplitude includes changes in speed and direction.

Table 1. Robot stability test (numerical simulation analysis)

Terrain Environment	Flat Ground	Slope	Smooth Surface	Flat Ground	Smooth Surface	Slope
Speed/Direction Change	0.5 m/s	15°	0.8 m/s	20°	1.0 m/s	30°
Initial Displacement (m)	0.1	0.2	0.15	0.1	0.12	0.3
Initial Orientation (°)	2	5	1.5	3	1	6
Stabilization Time (s)	2	3.2	2.3	3.5	1.9	4.1
Maximum Displacement Deviation (m)	0.12	0.18	0.1	0.25	0.08	0.2
Maximum Orientation Deviation (°)	3	4.5	2	4	2.2	3.5

On flat ground, when the robot encounters a speed disturbance of 0.5 m/s, the time required for recovery is 2 seconds, the maximum displacement deviation is 0.12 meters, and the maximum attitude deviation is 3°. When encountering a 20° directional disturbance, the stabilization time increases to 3.5 seconds, the maximum displacement deviation increases to 0.25 meters, and the maximum attitude deviation is 4°, indicating that directional disturbances have a greater impact on the stability of the robot. In contrast, in a ramp environment, when the robot is subjected to a 15° directional disturbance, the stabilization time is 3.2 seconds, the maximum displacement deviation is 0.18 meters, and the maximum attitude deviation is 4.5°. When the disturbance amplitude increases to 30°, the stabilization time is 4.1 seconds, the maximum displacement deviation is 0.2 meters, and the maximum attitude deviation is 3.5°. The robot in the ramp environment shows strong stability, especially under smaller disturbances. Finally, on smooth surfaces, the robot showed good recovery ability when facing speed disturbances, especially under 1.0 m/s speed disturbance, the recovery time is 1.9 seconds, the maximum displacement deviation is 0.08 meters, and the maximum posture deviation is 2.2°, indicating that the smooth surface had little effect on the robot's motion. Overall, the experimental results show that the robot's stability performance under different terrain conditions varies greatly, with better performance on ramps and smooth surfaces, while flat ground is more sensitive to directional disturbances.

5. Conclusion

This paper studies the engineering mechanics equations of a supported wheeled oil pipeline robot and proposes an optimized robot motion control model, aiming to solve the problem of poor

stability and adaptability of existing robots in complex pipeline environments. By constructing a detailed mechanical model, including factors such as normal force, tangential force and friction, this paper conducts an in-depth analysis of the dynamic response of the supported wheeled robot under different terrain conditions. The experimental results show that the supported wheeled robot based on the optimized mechanical model exhibits higher stability and lower motion error on the pipeline. When facing different slopes, curves and complex terrains, the robot's recovery ability and motion accuracy are significantly improved, and the maximum displacement deviation and posture deviation are significantly reduced. Especially in the case of high-speed movement and large slopes, the robot can maintain high motion stability and complete the task well. This study provides an important theoretical basis for the design and application of wheeled oil pipeline robots, and promotes the further development of pipeline robot technology in the field of intelligent inspection and maintenance. Future research can further explore adaptive control, path planning and other technologies based on existing mechanical models and control methods to cope with more complex pipeline environments and task requirements, thereby realizing the intelligent and efficient application of oil pipeline robot systems.

Acknowledgement

This work was supported by The Basic Research Business Expense Project of Autonomous Region Directly-Administered Universities in Inner Mongolia Autonomous Region, Project Number: GXKY22124.

References

[1] Nekoo S R, Acosta J Á, Ollero A. Combination of terminal sliding mode and finite-time state-dependent Riccati equation: Flapping-wing flying robot control[J]. Proceedings of the Institution of Mechanical Engineers, Part I: Journal of Systems and Control Engineering, 2023, 237(5): 870-887.

[2] Seghiri T, Ladaci S, Haddad S. Fractional order adaptive MRAC controller design for high-accuracy position control of an industrial robot arm[J]. International Journal of Advanced Mechatronic Systems, 2023, 10(1): 8-20.

[3] Semwal V B, Kim Y, Bijalwan V, et al. Development of the LSTM model and universal polynomial equation for all the sub-phases of human gait[J]. IEEE Sensors Journal, 2023, 23(14): 15892-15900.

[4] Armanini C, Boyer F, Mathew A T, et al. Soft robots modeling: A structured overview[J]. IEEE Transactions on Robotics, 2023, 39(3): 1728-1748.

[5] Briot S, Merlet J P. Direct kinematic singularities and stability analysis of sagging cable-driven parallel robots[J]. IEEE Transactions on Robotics, 2023, 39(3): 2240-2254.

[6] Kadhim R A, Kadhim M Q, Al-Khazraji H, et al. Bee algorithm based control design for two-links robot arm systems[J]. IIUM Engineering Journal, 2024, 25(2): 367-380.

[7] Ahmadizadeh M, Shafei A M, Fooladi M. Dynamic modeling of closed-chain robotic manipulators in the presence of frictional dynamic forces: A planar case[J]. Mechanics Based Design of Structures and Machines, 2023, 51(8): 4347-4367.

[8] Khorashadizadeh S, Zirkohi M M, Eliasi H, et al. Adaptive control of robot manipulators driven by permanent magnet synchronous motors using orthogonal functions theorem[J]. Journal of Vibration and Control, 2023, 29(11-12): 2789-2801.

[9] Lanh L A K, Duong V T, Nguyen H H, et al. Hybrid adaptive control for series elastic actuator of humanoid robot[J]. International Journal of Intelligent Unmanned Systems, 2023, 11(3): 359-377.

[10] Li W, Guo C, Ma X, et al. A strictly predefined-time convergent and noise-tolerant neural model for solving linear equations with robotic applications[J]. IEEE Transactions on Industrial Electronics, 2023, 71(1): 798-809.

[11] Barbosa A S, Tahara L Z, da Silva M M. Motion planning of a fish-like piezoelectric actuated robot using model-based predictive control[J]. Journal of Vibration and Control, 2023, 29(1-2): 411-427.

[12] Chotikunnan R, Roongprasert K, Chotikunnan P, et al. Robotic Arm Design and Control Using MATLAB/Simulink[J]. International Journal of Membrane Science and Technology, 2023, 10(3): 2448-2459.